

# Toward Highly Luminescent and Stabilized Silica-Coated Perovskite Quantum Dots through Simply Mixing and Stirring under Room Temperature in Air

Zheqin Liu,<sup>†,‡</sup> Yongqiang Zhang,<sup>\*,§</sup> Yi Fan,<sup>\*,†</sup> Zhenqiang Chen,<sup>§</sup> Zhaobing Tang,<sup>†,‡</sup> Jialong Zhao,<sup>§</sup> Ying Lv,<sup>†</sup> Jie Lin,<sup>†</sup> Xiaoyang Guo,<sup>†</sup> Jiahua Zhang,<sup>†</sup> and Xingyuan Liu<sup>\*,†</sup>

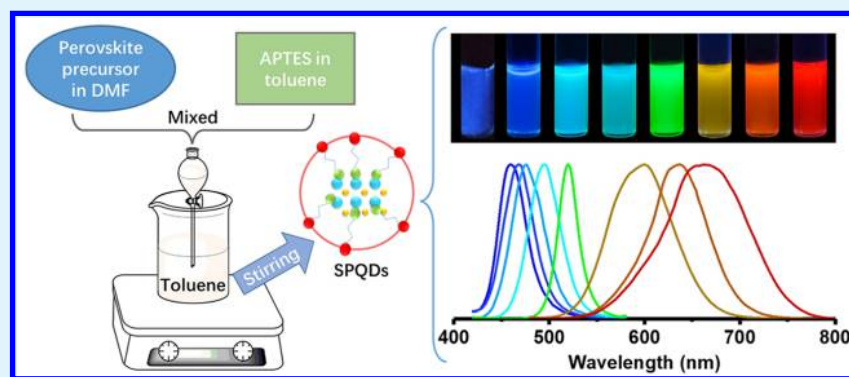
<sup>†</sup>State Key Laboratory of Luminescence and Applications, Changchun Institute of Optics, Fine Mechanics and Physics, Chinese Academy of Sciences, Changchun 130033, China

<sup>‡</sup>University of Chinese Academy of Sciences, Beijing 100039, China

<sup>§</sup>Department of Optoelectronic Engineering, Jinan University, Guangzhou 510632, China

<sup>§</sup>Key Laboratory of Functional Materials Physics and Chemistry of the Ministry of Education, Jilin Normal University, Siping 136000, China

## Supporting Information



**ABSTRACT:** Methylammonium (MA) lead halide (MAPbX<sub>3</sub>, X = Cl, Br, I) perovskite quantum dots (PQDs) are very sensitive to environment (moisture, oxygen, and temperature), suffering from poor stability. To improve the stability, we synthesized silica-coated PQDs (SPQDs) by an improved ligand-assisted reprecipitation method through simply mixing and stirring under room temperature in air without adding water and catalyst, the whole process took only a few seconds. The photoluminescence (PL) spectra of the SPQDs can be tuned continuously from 460 to 662 nm via adjusting the composition proportion of precursors. The highest PL quantum yields (PLQYs) of blue-, green-, and red-emissive SPQDs are 56, 95, and 70%, respectively. The SPQDs show remarkably improved environmental and thermal stability compared to the naked PQDs because of effective barrier created by the coated silica between the core materials and the ambience. Furthermore, it is found that different light-emitting SPQDs can maintain their original PL properties after mixing of them and anion-exchange reactions have not happened. These attributes were then used to mix green- and yellow-emissive SPQDs with polystyrene (PS) to form color-converting layers for the fabrication of white light-emitting devices (WLEDs). The WLEDs exhibit excellent white light characteristics with CIE 1931 color coordinates of (0.31, 0.34) and color rendering index (CRI) of 85, demonstrating promising applications of SPQDs in lighting and displays.

**KEYWORDS:** silane, silica-coated perovskite quantum dots, hydrolysis, stability, anion-exchange reaction

## INTRODUCTION

Conventional semiconductor quantum dots (QDs) have been widely used in various applications such as light-emitting diodes (LEDs), colloidal QD-based LEDs (QLEDs), solar cells, and bioimaging because of their excellent photoluminescence (PL) properties in terms of high PL quantum yield (PLQY), narrow spectral bandwidth, and tunable fluorescence emission.<sup>1–5</sup> In recent years, there has been an extended effort in developing new type of perovskite quantum dots (PQDs). In addition to the

above-mentioned advantages, there are some unique properties in PQDs compared with traditional QDs: better optical and charge transport properties, wider tunable spectral range, larger color gamut, simpler fabrication, lower cost, and lower synthesis temperature, which makes PQDs a promising candidate for optoelectronic devices.<sup>6–11</sup>

**Received:** December 13, 2017

**Accepted:** March 27, 2018

**Published:** March 27, 2018

However, their practical applications are hindered by the instability of PQDs. Specifically, when PQDs are exposed to surrounding environment, several factors such as moisture, oxygen, and high temperature will result in the structural degradation of PQDs and cause serious PL quenching, which is attributed to their high sensitivity to ambient conditions and strong ionic nature.<sup>12–14</sup> Moreover, the anion-exchange reactions between different PQDs when used together are still the major issues that obstruct their practical applications in multi-color display and lighting.<sup>15,16</sup>

A common method to circumvent these issues is the use of inorganic silica (SiO<sub>2</sub>) as coating agent to protect the inner materials from environmental degradation. Previous reports have shown that the stability of SiO<sub>2</sub>-coated QDs, such as CdSe-SiO<sub>2</sub>, ZnSe-SiO<sub>2</sub>, CdSe/ZnS-SiO<sub>2</sub>, and CdSe/CdS/ZnS-SiO<sub>2</sub>, are evidently improved.<sup>17–22</sup> Recently, Wang, Dirin, and Malgras et al. have formed perovskite/mesoporous silica composites by mixing PQDs with mesoporous silica or growing perovskite nanocrystals in mesoporous silica templates.<sup>23–26</sup> The as-prepared composites appeared somewhat stability. However, such composites are powdery materials with large amounts of silica, therefore it is detrimental to solution processing, which would limit their solution applications. In addition, the preparation of mesoporous silica is a complex process with high cost.

Hydrolysis of silane to form silica-coated QDs is a new method, which is controllable, low cost, easy to mass-produce and integrated with other applications. However, the hydrolysis reaction is water-assisted and thus leads to the fact that the PQDs will be decomposed by water before SiO<sub>2</sub> generation.<sup>27,28</sup> Despite the challenges, some research groups made appreciable contributions: Huang et al. added tetraethyl orthosilicate (TMOS) directly into PQD toluene solution and stirred for 36 h to fabricate a composite structure of PQDs wrapped with silica microspheres.<sup>29</sup> Luo et al. added (3-aminopropyl)triethoxysilane (APTES) while synthesizing PQDs under nitrogen atmosphere at 120–140 °C for 1 h and then stirred in air for 3 h at room temperature for hydrolysis of APTES to form QD/silica composite.<sup>30</sup> However, the above-mentioned processes are complicated and time-consuming, which require high temperature and prolonged stirring. Zhang's group used APTES as organic ligands and mixed them into N,N-dimethylformamide (DMF) solution of perovskite precursors for synthesizing APTES-capped PQDs by using traditional ligand-assisted reprecipitation method, but the highest PLQY of green QDs was only up to 55%, and the PLQY of the red PQDs was not described.<sup>31</sup> Therefore, it is desirable to synthesize silica coated PQDs (SPQDs) with high PLQY and high stability by a simple room-temperature procedure.

In this paper, we report a novel silica encapsulation process for PQDs, in which perovskite precursors are dissolved in DMF (analytical grade, H<sub>2</sub>O content ~0.1%), and APTES materials are dissolved in "waterless" toluene (analytical grade, H<sub>2</sub>O content ≤0.03%). APTES materials act as coating agent for the PQDs and the precursor of silica. Unlike previously reported one-pot method, which would cause premature hydrolysis of APTES before the formation of PQDs because DMF promotes the hydrolysis and leads to a large steric hindrance of the silane to the growth of perovskites and destroys the octahedral structure through N–Pb linkages.<sup>29</sup> The two solutions are quickly mixed and injected into vigorous stirring toluene solvent. The SPQDs can be synthesized in just a few seconds. Toluene is chosen as the solvent for its compatibility with both PQDs and APTES, and the very low-water content (≤0.03%). Such content of water would not cause decomposition of perovskites, but can provide an initial

condition for the hydrolysis of APTES. The system is open to the air and the trace water vapor is captured and reacted with APTES for deeper hydrolysis, which serves as an inexpensive and efficient preparation route. Through compositional modulations, PL emissions of the resulting SPQDs are readily tunable over the entire visible spectral region from 460 to 662 nm, the highest PLQYs of blue-, green- and red-emissive SPQDs were 56, 95, and 70%, respectively, which are in topped frontier level of reported PQDs, including all-inorganic ones. The SPQDs exhibited excellent stability after the silica encapsulation, and the anion-exchange reactions were not observed between different perovskite QDs, which are beneficial to fabricate white LEDs (WLEDs). By combining polystyrene (PS) and the green-, yellow-emissive SPQDs on a blue GaN LED chip, a WLED with Commission Internationale de l'Éclairage (CIE) 1931 color coordinates of (0.31, 0.34) and color rendering index (CRI) of 85 has been obtained, demonstrating their potential applications in white lighting and display.

## ■ MATERIALS AND METHODS

**Materials.** All reagents were used as received without further purification: toluene (AR, Beijing Chemical Works), dimethylformamide (DMF, AR, Beijing Chemical Works), (3-Aminopropyl)triethoxysilane (APTES, KH-550, 98%, Aladdin), (3-Mercaptopropyl)triethoxysilane (KH-580, 98%, Aladdin), 3-(2-Aminoethylamino)propyldimethoxymethylsilane (KH-602, 98%, Aladdin), oleic acid (OA, 90%, Alfa Aesar), lead(II) bromide (PbBr<sub>2</sub>, > 99.99%, Xi'an Polymer Light Technology Corp.), lead(II) iodide (PbI<sub>2</sub>, > 99.99%, Xi'an Polymer Light Technology Corp.), methylammonium bromide (MABr, > 99.5%, Xi'an Polymer Light Technology Corp.), methylammonium iodide (MAI, > 99.5%, Xi'an Polymer Light Technology Corp.), and polystyrene (PS, industrial grade), and deuteriochloroform (CDCl<sub>3</sub>, D.99.8%, TMS 0.03% v/v, Tenglong Weibo Technology Corp.).

**Synthesis of MAPbBr<sub>3</sub>/SiO<sub>2</sub> QDs.** For a typical method to synthesize MAPbBr<sub>3</sub> QDs coated with SiO<sub>2</sub> (MAPbBr<sub>3</sub>/SiO<sub>2</sub>(1:1), the molar ratio of Pb:Si = 1:1), 0.004 mmol PbBr<sub>2</sub> and 0.004 mmol MABr were dissolved in 100 μL of DMF, then 0.9 μL of APTES and 1 μL of oleic acid were dissolved in 1 μL of toluene. To synthesize MAPbBr<sub>3</sub>/SiO<sub>2</sub> QDs with different molar ratios of Pb:Si, we fixed the content of PbBr<sub>2</sub> and changed the volume of APTES proportionally. The precursors were then quickly mixed and injected into 2 mL of toluene solution under vigorous stirring (2500 rpm). The stirring was ongoing until the injection was finished, and the toluene solution then appeared in bright fluorescence under UV light irradiation. The entire process was controlled within a few seconds. All the above experiments were carried out at room temperature in atmosphere.

**Synthesis of MAPbBr<sub>x</sub>I<sub>3-x</sub>/SiO<sub>2</sub> QDs.** The detailed method to synthesize the mixed-anion MAPbBr<sub>x</sub>I<sub>3-x</sub> QDs coated with SiO<sub>2</sub> (MAPbBr<sub>x</sub>I<sub>3-x</sub>/SiO<sub>2</sub>) is as follows: 0.004 mmol of PbBr<sub>2</sub> (mixed with PbI<sub>2</sub> according to the proportion) and 0.004 mmol of MABr (mixed with MAI according to the proportion) were dissolved in 100 μL of DMF, then 2.7 μL of APTES and 1 μL of oleic acid were dissolved in 10 μL of toluene (the molar ratio of Pb:Si = 1:3, the amount of APTES was fixed by optimization (Figure S1)). The following procedure was the same as that of synthesis of MAPbBr<sub>3</sub>/SiO<sub>2</sub> QDs.

**Preparation of WLEDs.** To fabricate WLEDs, we uniformly mixed 0.16 mmol of MAPbBr<sub>3</sub>/SiO<sub>2</sub>(1:1.3) (green SPQDs, PLQY, 91%) and 0.16 mmol of MAPbBr<sub>1.05</sub>I<sub>1.95</sub>/SiO<sub>2</sub> (yellow SPQDs, PLQY, 60%) toluene solutions to form a 10 mL solution, 150 mg of PS was added and dissolved to form a homogeneous solution. The solution was then dropped on a commercially available blue chip and cured rapidly into film by natural evaporation of the solvents in air at room temperature. WLEDs can be fabricated by combining green/yellow dual fluorescent SPQDs/PS films and blue LED chips. All above operations were completed at room temperature in atmosphere.

**Characterizations.** Transmission electron microscope (TEM) and high resolution TEM (HRTEM) images were recorded with a FEI-TECNAI

G2 F30 TEM operating at 200 kV. Fourier Transform Infrared (FTIR) spectra were performed using KBr tablets with a Bio-Rad Excalibur FTS3000 spectrometer ( $4000\text{--}750\text{ cm}^{-1}$ ). X-ray diffraction (XRD) pattern was performed with a Bruker Advance D8 X-ray diffractometer. X-ray photoelectron spectra (XPS) were recorded on a Thermo Scientific ESCALAB 250 with Multitechnique Surface Analysis. UV/vis absorption spectra were measured on Shimadzu UV-3101 spectrophotometer. F-7000 Hitachi Fluorescence Spectrometer was used to record PL emission spectra. Fluorescence lifetimes were measured using FLS920 time-corrected single photon counting system. PLQYs were obtained in a calibrated integrating sphere in FLS920 spectrometer. The color coordinates and CCT of the WLEDs were measured on Ocean Optics USB-4000 Spectrometer. The  $^1\text{H}$ NMR spectra were measured with a Bruker AV-600 spectrometer. The preparation of APTES and  $\text{MAPbBr}_3/\text{SiO}_2$  QDs for the  $^1\text{H}$ NMR measurement is as follows:  $20\ \mu\text{L}$  APTES is dissolved in  $0.6\ \text{mL}$  of  $\text{CDCl}_3$  and  $0.64\ \text{mmol}$  of  $\text{MAPbBr}_3/\text{SiO}_2$  QDs are prepared as stated in the manuscript. After centrifugation, the precipitate is dissolved in  $0.6\ \text{mL}$  of  $\text{CDCl}_3$ .

## RESULTS AND DISCUSSION

Suitable ligands, such as *n*-octylamine and oleic acid, are often used to control the size and crystal phase of QDs and improve the PLQY.<sup>32–34</sup> According to Lewis acid–base theory, amino group as a Lewis base can react with a Lewis acid, such as  $\text{Pb}^{2+}$  ions, so does thiol group. Therefore, APTES (KH-550), (3-mercaptopropyl)-triethoxysilane (KH-580), and 3-(2-aminoethylamino)-propyldimethoxymethylsilane (KH-602), which contain  $-\text{NH}$  or  $-\text{SH}$  groups coupling with silane, are used as both coating agent for the PQDs and the precursor of silica in this work. Their condensed structural formulas are shown in Figure 1.

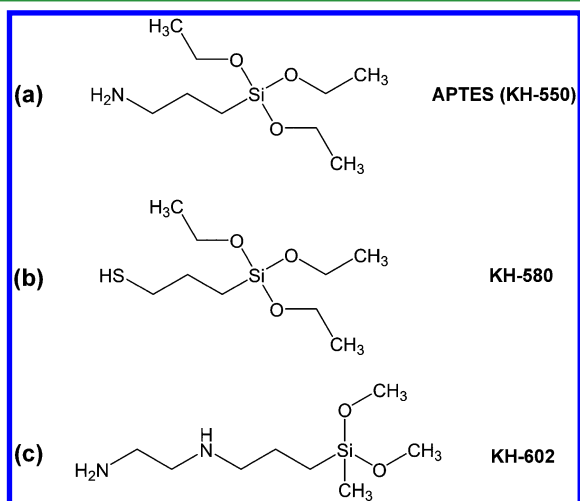


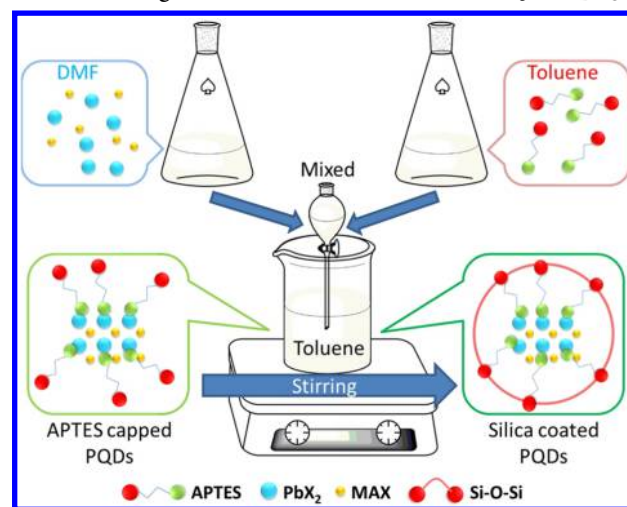
**Figure 1.** Condensed structural formula of (a) APTES, (b) KH-580, and (c) KH-602.

In our experiments, KH580 and KH602 resulted in severe quenching of perovskite. For KH580, thiol groups are easy to destroy the orthorhombic crystalline-phase perovskite at room temperature due to a great binding force with soft lead acid, leading to fluorescence quenching.<sup>35</sup> For KH602, methoxyl groups cause rapid hydrolysis, which in turn leads to the presence of large amounts of silica around the lead ions, so that hindering the growth of perovskite crystals.<sup>29</sup> Therefore, APTES is more suitable as a ligand for PQDs and silica precursors for further experiments.

In traditional ligand-assisted reprecipitation method, the precursor solution of PQDs and silane are usually dissolved in DMF. The DMF promotes the hydrolysis and results in increased steric hindrance of silane through the  $\text{N-Pb}$  linkage

to perovskite because of the strongly polar DMF can be connected to hydroxyl groups in  $\text{Si-OH}$  via hydrogen bonds.<sup>29,36</sup> Consequently, the linked silane would limit the growth of the perovskite and destroy the octahedral structure. The resulted SPQDs show low PLQYs.<sup>31</sup> Therefore, the traditional method needs to be developed to exclude the contact of silane with DMF in the precursor solution. To solve this issue, the precursors of perovskite ( $\text{MABr}$  and  $\text{PbBr}_2$ ) are dissolved in DMF, and APTES is dissolved in toluene, which can preclude the premature hydrolysis of APTES. The synthesis diagram is shown in Scheme 1.

**Scheme 1.** Diagram of the Formation of  $\text{MAPbX}_3/\text{SiO}_2$  QDs



During the synthesis, the two precursor solutions are quickly mixed with proper proportion and then rapidly injected into the vigorously stirring toluene solvent. The stirring is stopped as the injection completed. The toluene solution emits bright fluorescence under UV light irradiation. The entire process is controlled within a few seconds without the protection of inertial gas and high temperature.

The measured TEM reveals that  $\text{MAPbBr}_3/\text{SiO}_2(1:1)$  QDs are torispherical (Figure 2a) and clearly distinguished from the naked cubic PQDs (Figure S2).<sup>32–34</sup> As shown in the top inset of Figure 2a,  $\text{MAPbBr}_3/\text{SiO}_2(1:1)$  has a size distribution ranging from 1.6 to 3.8 nm with a mean value of around 2.57 nm. The size distribution is consistent with a Gaussian distribution. HRTEM (bottom inset of Figure 2a) reveals a highly ordered structure with the lattice spacing distance of 0.213 and 0.20 nm, which corresponds to in-plane lattice spacing of (200) and (330), and is consistent with the previous reports.<sup>32–34</sup> The XRD spectrum exhibits diffraction peaks at 14.8, 20.3, 29.7, 33.6, 42.7, and 45.5°, corresponding to interlayer spacing of (100), (110), (200), (210), (220), and (300) plane, which indicates the orthorhombic crystalline-phase (Figure 2b).<sup>32–35</sup> A broad peak around 20° corresponds to amorphous  $\text{SiO}_2$  (JCPDS card: 01–082–1554), which is similar to other silica-coated nanomaterials.<sup>36</sup> Surface functional groups are determined using FTIR (Figure 2c). The spectrum shows a broad O–H asymmetric stretching band from 3300 to 3600  $\text{cm}^{-1}$ , indicating successful capping and hydrolysis of APTES.<sup>31</sup> Bimodality around 1100  $\text{cm}^{-1}$  (1118 and 1075  $\text{cm}^{-1}$ ) and 766  $\text{cm}^{-1}$  peaks indicates the presence of  $\text{Si-O-Si}$  bonds. The peak at 943  $\text{cm}^{-1}$  is assigned to the  $\text{Si-OH}$  bond, which is generated from the hydrolysis of APTES, verifying the formation of a cross-linked organic silica network.<sup>37,38</sup> X-ray photoelectron spectroscopy (XPS) was carried out to determine the composition

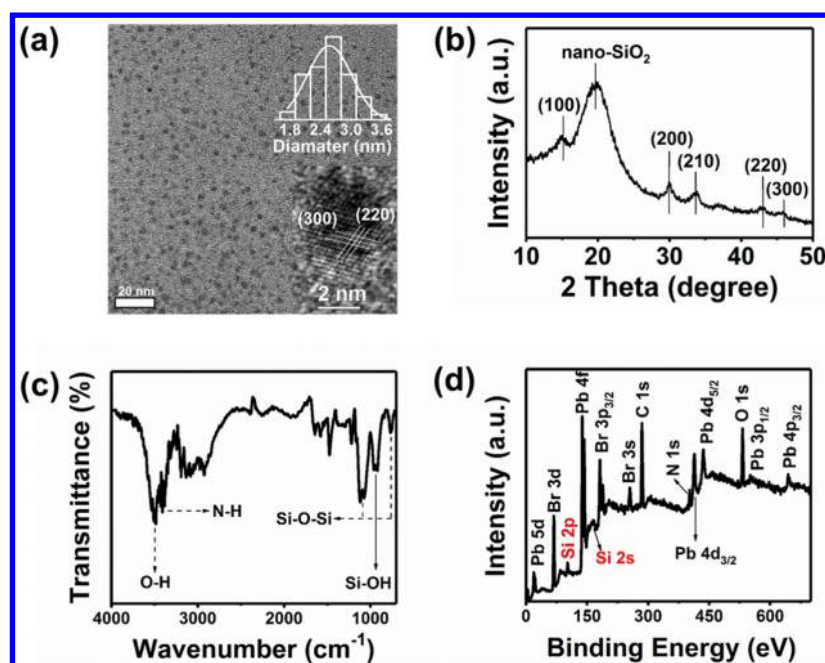
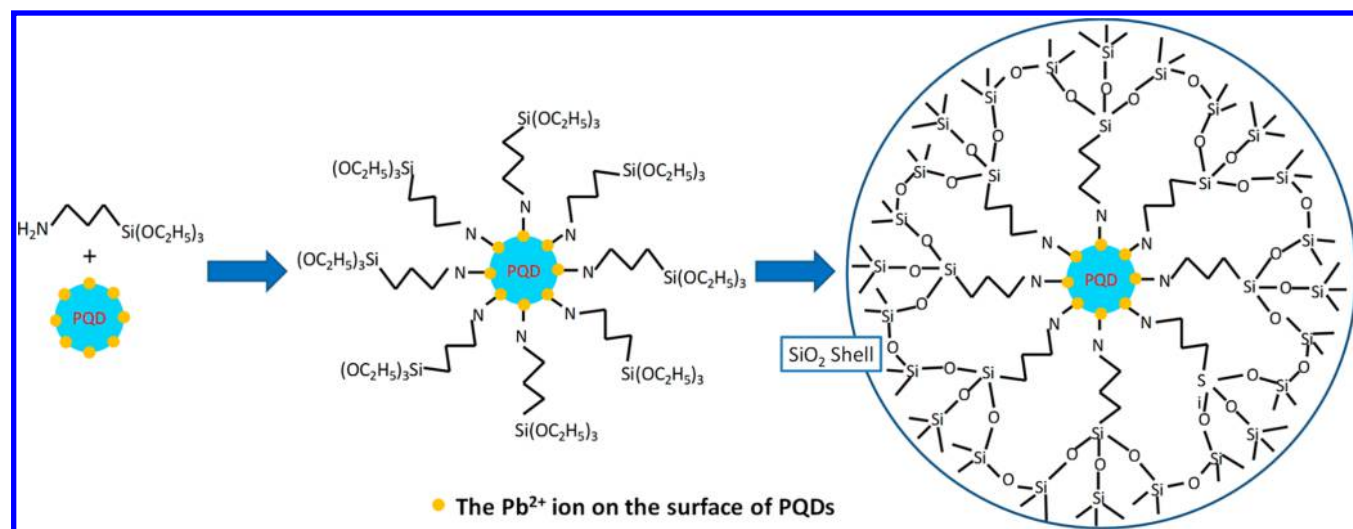


**Figure 2.** (a) Transmission electron microscopy (TEM) image, (the bottom inset is high-resolution TEM (HRTEM) image, the top inset is size distribution histogram), (b) X-ray diffraction (XRD) pattern, (c) Fourier transform infrared (FTIR) spectrum, and (d) X-ray photoelectron spectroscopy (XPS) full scan of MAPbBr<sub>3</sub>/SiO<sub>2</sub>(1:1) QDs.

### Scheme 2. Reaction Process Schematic of the Formation of SPQDs



of MAPbBr<sub>3</sub>/SiO<sub>2</sub>(1:1) QDs. As shown in Figure 2d and Figure S3, Si 2p at 102.3 eV and O 1s at 531.9 eV are consistent with the binding energies of SiO<sub>2</sub>, suggesting the formation of Si–O–Si bonds,<sup>39–41</sup> which is in agreement with the results of FTIR. The peak of 401.5 eV in N 1s indicates the presence of N as a charged species, which also suggests the interactions with PQDs surface.<sup>42,43</sup> The <sup>1</sup>HNMR spectra also illustrate the coordination of Pb(II) with –NH<sub>2</sub> as shown in Figure S4. It is well-known that the H atom in –NH<sub>2</sub> will be released when –NH<sub>2</sub> is combined to the metal ions. There are two proofs for the successful coordination of Pb(II) with –NH<sub>2</sub>. First, the chemical shift of –NH<sub>2</sub> totally disappears in SPQDs, while that in APTES is 7.293 ppm. This result indicates the release of H atom in –NH<sub>2</sub> group, which agrees well with the coordination procedure of –NH<sub>2</sub> group with Pb(II). Second, the chemical shift of –CH<sub>2</sub> (2.766 ppm) in SPQDs is increased compared to that in APTES (2.692 ppm),

which may be caused by the electron-pulling effect of coordinated Pb(II). Combined with the above two points, it will be safe to say that Pb(II) has been covalently coordinated with –NH<sub>2</sub> group. A schematic is used to describe the reaction process as shown in Scheme 2.

Surface organic ligands are well considered as a key factor in the synthesis of QDs. In order to obtain high PLQY SPQDs, the PL spectra of the MAPbBr<sub>3</sub>/SiO<sub>2</sub> QDs synthesized with different molar ratios of Pb:Si were examined. The embedding of a suitable organic ligand usually increases the coordination numbers of the metal atoms inside the QDs and effectively reduces the energy states of the surface dangling bonds. Such energy states are considered as nonradiative recombination centers. These ligands that do not directly participate in the bandgap structure of the QDs can affect the growth process of QDs, leading to changes in their final PL properties.<sup>44</sup>

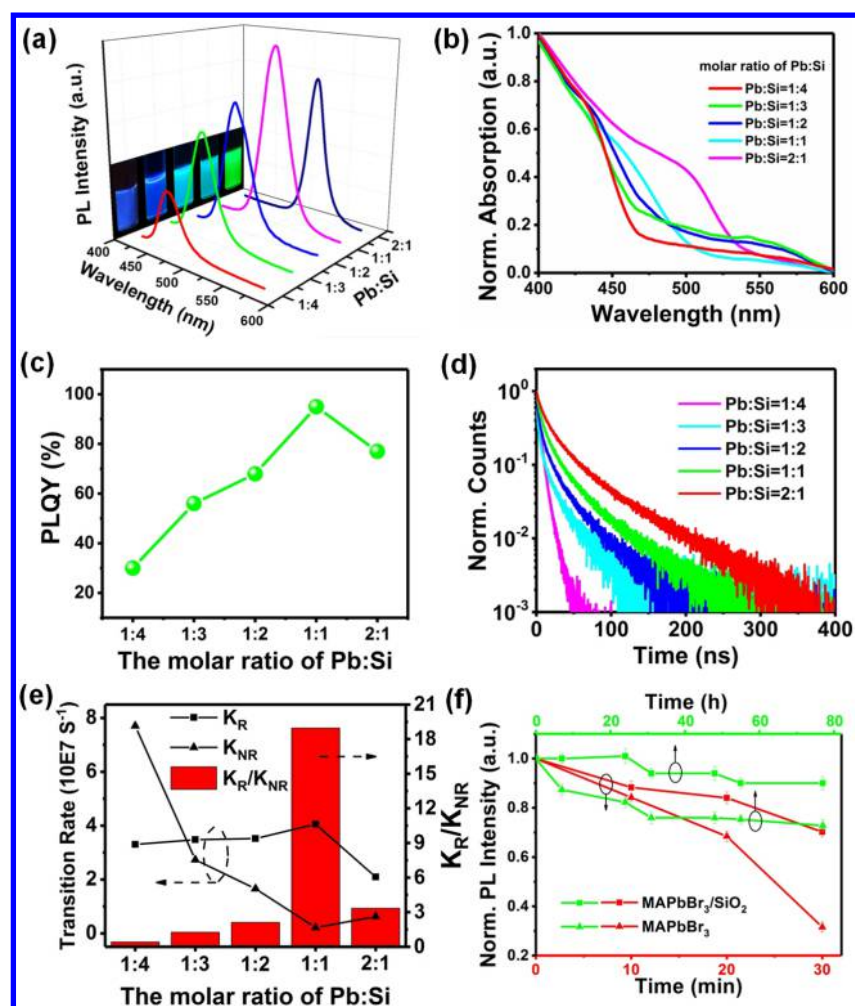


**Figure 3.** (a) Digital picture and PL spectra of MAPbBr<sub>3</sub>/SiO<sub>2</sub> QDs with different molar ratios of Pb:Si under illumination of 365 nm light; (b) absorption spectra of MAPbBr<sub>3</sub>/SiO<sub>2</sub> QDs; (c) PLQYs of MAPbBr<sub>3</sub>/SiO<sub>2</sub> QDs with different molar ratio of Pb:Si; (d) PL decay curves of MAPbBr<sub>3</sub>/SiO<sub>2</sub> QDs; (e) radiative transition rates ( $K_R$ ), nonradiative transition rates ( $K_{NR}$ ), and  $K_R/K_{NR}$  of MAPbBr<sub>3</sub>/SiO<sub>2</sub> QDs; (f) air (green) and thermal (red) stability comparison of MAPbBr<sub>3</sub>/SiO<sub>2</sub>(1:1) QDs with MAPbBr<sub>3</sub> QDs.

As can be seen in Figure 3a, varying the Pb:Si molar ratio in the precursor, the prepared MAPbBr<sub>3</sub>/SiO<sub>2</sub> QDs show different emission colors ranging from blue to green under 365 nm excitation. The emission peaks locates at 460, 468, 475, 495, and 520 nm while the Pb:Si ratio equals to 1:4, 1:3, 1:2, 1:1, and 2:1, respectively. As the ratio of Pb:Si increases, the PL peak and the absorption spectra red shifts (Figure 3a, b). In fact, the size-dependent PL properties are ubiquitous in the field of QDs. Particularly, in a same system, the longer the wavelength, the larger its size. For example, it is difficult to centrifuge the SPQDs (Pb:Si = 1:4) even at 15 000 rpm speed, but the SPQDs with Pb:Si ratio equals to 1:1 can be centrifuged with the speed rate of 3000 rpm easily, indicates that the size of MAPbBr<sub>3</sub>/SiO<sub>2</sub>(1:4) is much smaller than that of MAPbBr<sub>3</sub>/SiO<sub>2</sub>(1:1), which is in perfect accordance with the PL wavelengths. The PLQYs corresponding to MAPbBr<sub>3</sub>/SiO<sub>2</sub>(1:4), MAPbBr<sub>3</sub>/SiO<sub>2</sub>(1:3), MAPbBr<sub>3</sub>/SiO<sub>2</sub>(1:2), MAPbBr<sub>3</sub>/SiO<sub>2</sub>(1:1), and MAPbBr<sub>3</sub>/SiO<sub>2</sub>(2:1) are 30, 56, 68, 95, and 77%, respectively (Figure 3c), whereas the PLQY of naked MAPbBr<sub>3</sub> QDs (use n-octylamine and oleic acid as ligands, the same as other reports<sup>32–34</sup>) is 96%. It is worth noting that the highest PLQY of green-emissive QDs (95%) is 1.7 folds of that of the QDs synthesized by traditional method.<sup>31</sup> The coated silica plays a key role in controlling the growth and defects of PQDs. In the synthesis of MAPbBr<sub>3</sub>/SiO<sub>2</sub> QDs, the content of lead is

fixed. While the ratio of Pb:Si changes from 1:1 to 1:4, the numbers of APTES linked to a single Pb atom on the surface of SPQDs gradually increases, and the spatial steric hindrance caused by hydrolysis of APTES strengthens. Such steric hindrance limits the growth of perovskite and bring on defects, so the size of the PQDs will decrease and the defects increase with the addition of APTES,<sup>45,46</sup> thus PLQY declines. When the molar ratio of Pb:Si exceeds 1:1 and continues to increase, PQDs grow, whereas the small amount of organic silica is insufficient to coat the dangling bonds and defects exposed on the surface of the PQDs, thereby reducing PLQY. In a word, too much or too little APTES will lead to a low PLQY. To investigate the mechanism behind the high PLQY, we obtained the PL decay curves of these SPQDs (Figure 3d). The fitting results with biexponential functions are shown in Table S1. The average PL lifetimes are estimated using eq 1.<sup>47</sup>

$$\tau_{av} = \frac{\sum_i A_i \tau_i^2}{\sum_i A_i \tau_i} \quad (1)$$

Here,  $\tau_i$  and  $A_i$  are the time components and weights of the multiple exponential functions used for analyzing the PL decay curves, respectively.  $\tau_{av}$  of MAPbBr<sub>3</sub>/SiO<sub>2</sub>(2:1), MAPbBr<sub>3</sub>/SiO<sub>2</sub>(1:1), MAPbBr<sub>3</sub>/SiO<sub>2</sub>(1:2), MAPbBr<sub>3</sub>/SiO<sub>2</sub>(1:3), and

MAPbBr<sub>3</sub>/SiO<sub>2</sub>(1:4) are 36.73, 23.41, 19.31, 16.08, and 9.08 ns respectively, which decreases with the reduction of Pb:Si. Radiative transition rate ( $K_R$ ) and nonradiative transition rate ( $K_{NR}$ ) can be obtained from lifetime and PLQY by using eqs 2 and 3.<sup>48</sup>

$$\tau_{av} = (K_R + K_{NR})^{-1} \quad (2)$$

$$\Phi = K_R(K_R + K_{NR})^{-1} \quad (3)$$

Where,  $\Phi$  is the PLQY and  $\tau_{av}$  is the average excited state lifetime.  $\tau_{av}$  and  $\Phi$  can be further deduced from eqs 2 and 3:

$$\tau_{av} = \Phi/K_R \quad (4)$$

$$\Phi = \frac{1}{1 + \frac{K_{NR}}{K_R}} \quad (5)$$

For different QDs, neither PLQY and  $K_R$  are fixed numbers. In MAPbBr<sub>3</sub>/SiO<sub>2</sub>(2:1) QDs, small amounts of organic silica is insufficient to passivate the surface defects. Thus, increased surface defects in MAPbBr<sub>3</sub>/SiO<sub>2</sub>(2:1) QDs can be expected and lead to an increased  $K_{NR}/K_R$  and a decreased PLQY, which is in accordance with the measured PLQY results (The PLQYs of MAPbBr<sub>3</sub>/SiO<sub>2</sub>(1:1) and MAPbBr<sub>3</sub>/SiO<sub>2</sub>(2:1) are 95 and 70%, respectively). The  $K_R$  and  $K_{NR}$  can be obtained from the measured  $\Phi$  and  $\tau$  (as shown in Table S2 and Figure 3e), which are  $4.06 \times 10^7 \text{ s}^{-1}$  and  $0.21 \times 10^7 \text{ s}^{-1}$  for MAPbBr<sub>3</sub>/SiO<sub>2</sub>(1:1), and  $2.10 \times 10^7 \text{ s}^{-1}$  and  $0.63 \times 10^7 \text{ s}^{-1}$  for MAPbBr<sub>3</sub>/SiO<sub>2</sub>(2:1). The total change of  $K_R$  and  $K_{NR}$  results in a longer lifetime in MAPbBr<sub>3</sub>/SiO<sub>2</sub>(2:1). Recently, it is found that the PL of PQDs originates not only from recombination of exciton, but also from the thermally activated defects or traps below the conduction band, which would prolong the lifetime of excited states.<sup>49–51</sup> Therefore, it would be possible that surface defects in MAPbBr<sub>3</sub>/SiO<sub>2</sub> QDs have effects on both the proportion of  $K_{NR}$  to  $K_R$ , and the PL lifetime of QDs. The discrepancy of PLQY and PL lifetime were also shown in previous reports.<sup>32,52</sup> In a word, there is no positive or negative correlation between PLQY and PL lifetime. According to eq 5, the PLQY is generally proportional to  $K_R/K_{NR}$ . The resulting  $K_R/K_{NR}$  ratios of the MAPbBr<sub>3</sub>/SiO<sub>2</sub>(2:1), MAPbBr<sub>3</sub>/SiO<sub>2</sub>(1:1), MAPbBr<sub>3</sub>/SiO<sub>2</sub>(1:2), MAPbBr<sub>3</sub>/SiO<sub>2</sub>(1:3), and MAPbBr<sub>3</sub>/SiO<sub>2</sub>(1:4) are 3.34, 18.96, 2.12, 1.27, and 0.43, respectively, which basically match the PLQYs curve. This is in agreement with the previous report that silica coated QDs with higher PLQY owns more excitonic radiative transitions than that of other QDs with low PLQY.<sup>32</sup>

The coated SiO<sub>2</sub> can effectively prevent the inner perovskite from contacting air and moisture, and improve the stability.<sup>29,53</sup> To verify the stability, MAPbBr<sub>3</sub>/SiO<sub>2</sub>(1:1) and naked MAPbBr<sub>3</sub> were placed in ambient atmosphere at room temperature, their PL intensities were measured at intervals. As shown in the top X axis of Figure 3f, the emission intensity of the SPQDs is reduced by only 6% after 72 h, whereas that of the naked PQDs is reduced by 36%. Their thermal stabilities were also compared under 60 °C lasted for 30 min (bottom X axis). The emission intensity of SPQDs is decreased by 34%, whereas that of the naked PQDs is almost quenched. Heating exacerbate the decomposition of the naked PQDs while in contact with water and oxygen in the air. These results show that the coating silica significantly improves the air and thermal stability of the inner perovskite. On the other hand, the coated silica will also increase the resistance of polar solvent. Different volume of ethanol was added into 2 mL naked PQDs and SPQDs solution for comparing their PL spectra. As shown in Figure S5, 0.6 mL of

ethanol leads to serious PL quenching of naked MAPbBr<sub>3</sub> QDs, whereas the PL intensity of MAPbBr<sub>3</sub>/SiO<sub>2</sub> is only reduced by half, and 1 mL of ethanol reduces the PL intensity to one-third. It shows that PQDs coated with SiO<sub>2</sub> have better resistance of polar solvent than PQDs without SiO<sub>2</sub> encapsulation.

Similar to traditional PQDs, the emission wavelength of SPQDs can also be tuned by changing the ratio of halide in the precursor. TEM image illustrated that MAPbBr<sub>0.45</sub>I<sub>2.55</sub>/SiO<sub>2</sub> QDs are quasi-spherical and uniformly distributed without aggregation (Figure S6). Figures S7 and S8 are FTIR and XPS spectra of MAPbBr<sub>0.45</sub>I<sub>2.55</sub>/SiO<sub>2</sub> QDs, respectively. Both of them demonstrate the successful hydrolysis of APTES and the formation of a cross-linked silica coating. Figure 4a shows the digital photos of MAPbBr<sub>x</sub>I<sub>3-x</sub>/SiO<sub>2</sub> QDs and their corresponding PL spectra. With the decrease of the Br:I in the precursor, the fluorescence of SPQDs is changed from yellow to red. The content of I<sup>-</sup> accounts for 70% (MAPbBr<sub>0.9</sub>I<sub>2.1</sub>/SiO<sub>2</sub>), 85% (MAPbBr<sub>0.45</sub>I<sub>2.55</sub>/SiO<sub>2</sub>), and 100% (MAPbI<sub>3</sub>/SiO<sub>2</sub>), their corresponding PL peaks located at 600, 635, and 662 nm, respectively, and their PLQYs were measured to be 62%, 70% and 48% (Figure S9), whereas the PLQY of naked MAPbBr<sub>0.45</sub>I<sub>2.55</sub> QDs is 72%. The UV/vis absorption peaks are located at 548, 570, and 603 nm, respectively, and red-shifted as the content of I<sup>-</sup> increased (Figure 4b).

The PL decay curves of the MAPbBr<sub>x</sub>I<sub>3-x</sub>/SiO<sub>2</sub> QDs are fitted well with biexponential functions and the results are shown in Table S3. The average lifetimes of MAPbBr<sub>0.9</sub>I<sub>2.1</sub>/SiO<sub>2</sub>, MAPbBr<sub>0.45</sub>I<sub>2.55</sub>/SiO<sub>2</sub> and MAPbI<sub>3</sub>/SiO<sub>2</sub> QDs are 8.88, 12.94, and 21.03 ns by using eq 1, respectively.  $K_R$  and  $K_{NR}$  were calculated and shown in Table S4 and Figure 4c (using eqs 2 and 3). The  $K_R/K_{NR}$  values of MAPbBr<sub>0.9</sub>I<sub>2.1</sub>/SiO<sub>2</sub>, MAPbBr<sub>0.45</sub>I<sub>2.55</sub>/SiO<sub>2</sub>, and MAPbI<sub>3</sub>/SiO<sub>2</sub> are 1.59, 2.03, and 0.92, respectively, which match the PLQY tendency (Figure S9). Similar to MAPbBr<sub>3</sub>/SiO<sub>2</sub> QDs, the SiO<sub>2</sub> prevented the MAPbBr<sub>x</sub>I<sub>3-x</sub>/SiO<sub>2</sub> QDs from contacting with air and moisture, so as to improve the stability of the QDs. As shown in Figure 4d, after 15 min-heating at 60 °C in the atmosphere, the emission intensity of the SPQDs is reduced by 25% and that of the naked QDs is reduced by 46%, which demonstrate that the SPQDs have better thermal stability than naked ones.

The fluorescence quality of PQDs is superior to other QDs to some extent, such as wider tunable spectral range, wider color gamut and narrower bandwidth. These properties make PQDs of potential applications in multicolor display and white lighting. While, PQDs cannot be simply mixed to produce a colorful light as conventional QDs do, because anion-exchange reactions occur rapidly among different PQDs.<sup>15</sup> As shown in Figure S10a, only one peak of 576 nm is observed after the mixture of naked MAPbBr<sub>3</sub> QDs with the PL peak at 520 nm and naked MAPbBr<sub>0.45</sub>I<sub>2.55</sub> QDs with the PL peak at 613 nm. The normalized PL spectra of the synthesized MAPbBr<sub>3</sub>/SiO<sub>2</sub> and MAPbBr<sub>0.45</sub>I<sub>2.55</sub>/SiO<sub>2</sub> QDs were measured before and after their mixture (Figure S10b). As can be seen, the mixture still retains the two original PL peaks from the two components, indicating that the coated silica can prevent the rapid anion-exchange reactions. Besides, the mixed SPQDs still shows high stability under long-term storage of 24 h (Figure S11). Thus, luminescent SPQDs can be potentially applied to commercial WLEDs based on a blue-emitting LED chip.

Green- (508 nm) and yellow-emissive (588 nm) SPQDs solution were mixed in proper proportion, then PS was added and dissolved to form a homogeneous and viscous solution, the mixture was dropped and applied evenly onto commercially available blue GaN LEDs, then cured rapidly into film at room temperature

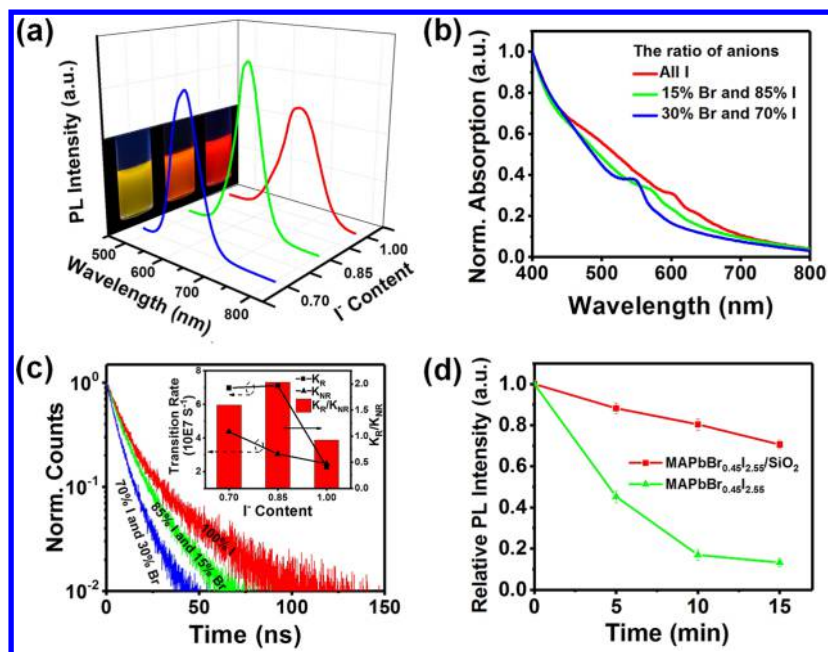


**Figure 4.** (a) Digital picture and the PL spectra of MAPbBr<sub>1-x</sub>I<sub>x</sub>/SiO<sub>2</sub> QDs with different I<sup>-</sup> contents; (b) absorption and PL spectra of MAPbBr<sub>0.45</sub>I<sub>2.55</sub>/SiO<sub>2</sub> QDs; (c) PL decay curves of MAPbBr<sub>0.45</sub>I<sub>2.55</sub>/SiO<sub>2</sub> QDs, the inset is the  $K_R$ ,  $K_{NR}$ , and  $K_R/K_{NR}$  of MAPbBr<sub>0.45</sub>I<sub>2.55</sub>/SiO<sub>2</sub> QDs; (d) thermal stability of MAPbBr<sub>0.45</sub>I<sub>2.55</sub>/SiO<sub>2</sub> QDs and MAPbBr<sub>0.45</sub>I<sub>2.55</sub> QDs.

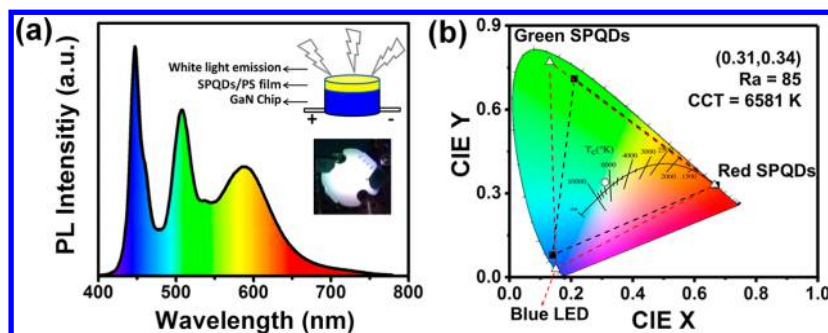


**Figure 5.** (a) PL spectrum of the working WLED (top inset, schematic diagram of the WLED device; bottom inset, the photograph of the device under working). (b) Color triangle of the blue LED, the green and red SPQDs (red dashed line) compared to the NTSC TV standard (black dashed line) and the CIE color coordinates of the WLED device.

by natural evaporation of the solvents in air at room temperature. The films exhibit dual fluorescence emission with green and yellow color, preserving the original PL characteristics. This is superior to conventional inorganic bulk phosphors, whose fluorescence property is often impaired after grinding process (generating defects on their host lattice).<sup>54</sup> As a result, WLEDs were fabricated by combining green/yellow dual fluorescent SPQDs/PS films and blue LED chips. As shown in Figure 5a, the top inset is the schematic diagram of the WLED device, the bottom inset is the working device photo. The WLED shows a white light spectrum under working with three discrete emission peaks located at 447, 508, and 588 nm, originating from blue-chip, green and yellow SPQDs, respectively. No intermediate emission peaks were detected, revealing that the QDs are well embedded in silica and the anion exchange reactions between them are successfully blocked. Figure 5b shows that the WLED device has a white lighting color coordinates of (0.31, 0.34), a color rendering index (CRI) of 85, and a color temperature of 6581 K. Notably, the CIE 1931 color coordinates of the blue chip, green and red SPQDs constitute a wide color gamut as high as 121% of the National Television System Committee (NTSC)

1953 color space standard, which is better than other QDs,<sup>55–57</sup> demonstrating a great potential application of SPQDs in displays and white-lighting. The highest luminous efficiency of the WLED was measured and shown in Figure S12. The highest power efficiency reached 54 lm/W, which is higher than the CdSe QD/silica monolith.<sup>58</sup> The power efficiency was not optimized; it could be further improved by increasing the chip efficiency, optimizing the structure and reducing the scattering of the light.

## CONCLUSIONS

In summary, SPQDs were synthesized using an improved silane ligand-assisted reprecipitation method in air at room temperature. By precisely controlling the proportion of the precursors, the emission wavelength can be tuned from 460 to 662 nm. The highest PLQY of blue, green, and red of SPQDs are 56, 95, and 70%, respectively, which are in topped frontier level of PQDs, including all-inorganic ones. SPQDs exhibit significantly improved environmental stability compared to the naked PQDs, and the different SPQDs can keep their original PL properties after mixture without changing the spectra caused by rapid anion-exchange. Our work provides a simple and generally applicable

pathway to synthesize highly luminescent and stabilized SPQDs. Moreover, WLEDs were realized by using the mixture films of PS, green and yellow SPQDs combined with blue GaN LEDs. The obtained WLEDs show nice white light color coordinates, color rendering index, and a wide color gamut. We believe that this new kind of SPQDs would have significant applications in the fields of displays, lighting, photodetectors, and lasers.

## ■ ASSOCIATED CONTENT

### Supporting Information

The Supporting Information is available free of charge on the ACS Publications website at DOI: 10.1021/acsami.7b18964.

Synthesis of naked MAPbX<sub>3</sub> QDs, optimization of APTES, TEM image, XPS spectra, <sup>1</sup>HNMR spectra, PL spectra against polar solvent, lifetime results, radiative transition rates and nonradiative transition rates, FTIR spectrum, PLQY, PL spectra before and after mixture, PL spectra of the mixture exposed for long-term in air, power efficiency of WLED device (PDF)

## ■ AUTHOR INFORMATION

### Corresponding Authors

\*E-mail: zhangyongqiang@jnu.edu.cn (Y.Z.).

\*E-mail: fanyi@ciomp.ac.cn (Y.F.).

\*E-mail: liuxy@ciomp.ac.cn (X.L.).

### ORCID

Yi Fan: 0000-0003-0379-9842

Jialong Zhao: 0000-0001-9020-1436

Ying lv: 0000-0003-1649-5258

Jie Lin: 0000-0001-9676-2218

Xiaoyang Guo: 0000-0003-0259-137X

Xingyuan Liu: 0000-0002-9681-1646

### Notes

The authors declare no competing financial interest.

## ■ ACKNOWLEDGMENTS

This work is supported by the CAS Innovation Program, the National Natural Science Foundation of China 61774154, 51503196, and 61405195; the Jilin Province Science and Technology Research Project 20170101039JC, 20150101039JC, 20160520176JH, and 20160520092JH; and project supported by State Key Laboratory of Luminescence and Applications.

## ■ REFERENCES

- (1) Shirasaki, Y.; Supran, G. J.; Bawendi, M. G.; Bulovic, V. Emergence of Colloidal Quantum-dot Light-emitting Technologies. *Nat. Photonics* **2013**, *7*, 13–23.
- (2) Kovalenko, M. V.; Manna, L.; Cabot, A.; Hens, Z.; Talapin, D. V.; Kagan, C. R.; Klimov, V.; Rogach, A. L.; Reiss, P.; Milliron, D. J.; Guyot-Sionnest, P.; Konstantatos, G.; Parak, W. J.; Hyeon, T.; Korgel, B. A.; Murray, C. B.; Heiss, W. Prospects of Nanoscience with Nanocrystals. *ACS Nano* **2015**, *9*, 1012–1057.
- (3) Wang, Y.; Li, X.; Song, J.; Xiao, L.; Zeng, H.; Sun, H. All-Inorganic Colloidal Perovskite Quantum Dots: A New Class of Lasing Materials with Favorable Characteristics. *Adv. Mater.* **2015**, *27*, 7101–7108.
- (4) Dai, X. L.; Zhang, Z. X.; Jin, Y. Z.; Niu, Y.; Cao, H. J.; Liang, X. Y.; Chen, L. W.; Wang, J. P.; Peng, X. G. Solution-processed, High-Performance Light-Emitting Diodes Based on Quantum Dots. *Nature* **2014**, *515*, 96–99.
- (5) Lee, K. H.; Lee, J. H.; Kang, H. D.; Park, B.; Kwon, Y.; Ko, H.; Lee, C.; Lee, J.; Yang, H. Over 40 cd/A Efficient Green Quantum Dot

Electroluminescent Device Comprising Uniquely Large-sized Quantum Dots. *ACS Nano* **2014**, *8*, 4893–4901.

- (6) Ning, Z.; Gong, X.; Comin, R.; Walters, G.; Fan, F.; Voznyy, O.; Yassitepe, E.; Buin, A.; Hoogland, S.; Sargent, E. H. Quantum-dot-in-perovskite solids. *Nature* **2015**, *523*, 324–328.

- (7) Berry, J.; Buonassisi, T.; Egger, D. A.; Hodes, G.; Kronik, L.; Loo, Y.; Lubomirsky, I.; Marder, S. R.; Mastai, Y.; Miller, J. S.; Mitzi, D. B.; Paz, Y.; Rappe, A. M.; Riess, I.; Rybtchinski, B.; Stafsudd, O.; Stevanovic, V.; Toney, M. F.; Zitoun, D.; Kahn, A.; Ginley, D.; Cahen, D. Hybrid Organic-Inorganic Perovskites (HOIPs): Opportunities and Challenges. *Adv. Mater.* **2015**, *27*, 5102–5112.

- (8) Fang, H.; Raissa, R.; Abdu-Aguye, M.; Adjokatsé, S.; Blake, G.; Even, J.; Loi, M. Hybrid Perovskites: Photophysics of Organic-Inorganic Hybrid Lead Iodide Perovskite Single Crystals. *Adv. Funct. Mater.* **2015**, *25*, 2378–2385.

- (9) Zhou, Q. C.; Bai, Z. L.; Lu, W. G.; Wang, Y. T.; Zou, B. S.; Zhong, H. Z. In Situ Fabrication of Halide Perovskite Nanocrystal-Embedded Polymer Composite Films with Enhanced Photoluminescence for Display Backlights. *Adv. Mater.* **2016**, *28*, 9163–9168.

- (10) Deng, W.; Xu, X.; Zhang, X.; Zhang, Y.; Jin, X.; Wang, L.; Lee, S.; Jie, J. Organometal Halide Perovskite Quantum Dot Light-Emitting Diodes. *Adv. Funct. Mater.* **2016**, *26*, 4797–4802.

- (11) Im, J. H.; Lee, C. R.; Lee, J. W.; Park, S. W.; Park, N. G. 6.5% efficient perovskite quantum-dot-sensitized solar cell. *Nanoscale* **2011**, *3*, 4088–4093.

- (12) Schmidt, L. C.; Pertegás, A.; González-Carrero, S.; Malinkiewicz, O.; Agouram, S.; Minguez Espallargas, G.; Bolink, H. J.; Galian, R. E.; Pérez-Prieto, J. Nontemplate Synthesis of CH<sub>3</sub>NH<sub>3</sub>PbBr<sub>3</sub> Perovskite Nanoparticles. *J. Am. Chem. Soc.* **2014**, *136*, 850–853.

- (13) Raja, S. N.; Bekenstein, Y.; Koc, M. A.; Fischer, S.; Zhang, D.; Lin, L.; Ritchie, R. O.; Yang, P.; Alivisatos, A. P. Encapsulation of Perovskite Nanocrystals into Macroscale Polymer Matrices: Enhanced Stability and Polarization. *ACS Appl. Mater. Interfaces* **2016**, *8*, 35523–35533.

- (14) Pan, J.; Sarmah, S. P.; Murali, B.; Dursun, I.; Peng, W.; Parida, M. R.; Liu, J.; Sinatra, L.; Alyami, N.; Zhao, C.; Alarousu, E.; Ng, T. K.; Ooi, B. S.; Bakr, O. M.; Mohammed, O. F. Air-Stable Surface-Passivated Perovskite Quantum Dots for Ultra-Robust, Single- and Two-Photon-Induced Amplified Spontaneous Emission. *J. Phys. Chem. Lett.* **2015**, *6*, 5027–5033.

- (15) Nedelcu, G.; Protesescu, L.; Yakunin, S.; Bodnarchuk, M. I.; Grotevent, M. J.; Kovalenko, M. V. Fast Anion-Exchange in Highly Luminescent Nanocrystals of Cesium Lead Halide Perovskites (CsPbX<sub>3</sub>, X = Cl, Br, I). *Nano Lett.* **2015**, *15*, 5635–5640.

- (16) Akkerman, Q. A.; D'Innocenzo, V.; Accornero, S.; Scarpellini, A.; Petrozza, A.; Prato, M.; Manna, L. Tuning the Optical Properties of Cesium Lead Halide Perovskite Nanocrystals by Anion Exchange Reactions. *J. Am. Chem. Soc.* **2015**, *137*, 10276–10281.

- (17) Selvan, S. T.; Tan, T. T.; Ying, J. Y. Robust, Non-Cytotoxic, Silica-Coated CdSe Quantum Dots with Efficient Photoluminescence. *Adv. Mater.* **2005**, *17*, 1620–1625.

- (18) Zhang, T.; Stilwell, J. L.; Gerion, D.; Ding, L.; Elboudwarej, O.; Cooke, P. A.; Gray, J. W.; Alivisatos, A. P.; Chen, F. F. Cellular Effect of High Doses of Silica-Coated Quantum Dot Profiled with High Throughput Gene Expression Analysis and High Content Cellomics Measurements. *Nano Lett.* **2006**, *6*, 800–808.

- (19) Anderson, B. D.; Wu, W. C.; Tracy, J. B. Silica Overcoating of CdSe/CdS Core/Shell Quantum Dot Nanorods with Controlled Morphologies. *Chem. Mater.* **2016**, *28*, 4945–4952.

- (20) Zhao, F.; Zheng, J. G.; Yang, X.; Li, X.; Wang, J.; Zhao, F.; Wong, K. S.; Liang, C.; Wu, M. Complex ZnO Nanotree Arrays with Tunable Top, Stem and Branch Structures. *Nanoscale* **2010**, *2*, 1674–1683.

- (21) Jun, S.; Lee, J.; Jang, E. Highly Luminescent and Photostable Quantum Dot-Silica Monolith and Its Application to Light-Emitting Diodes. *ACS Nano* **2013**, *7*, 1472–1477.

- (22) Zhao, B.; Yao, Y.; Gao, M.; Sun, K.; Zhang, J.; Li, W. Doped Quantum Dot@Silica Nanocomposites for White Light-emitting Diodes. *Nanoscale* **2015**, *7*, 17231–17236.

- (23) Wang, H. C.; Lin, S. Y.; Tang, A. C.; Singh, B. P.; Tong, H. C.; Chen, C. Y.; Lee, Y. C.; Tsai, T. L.; Liu, R. S. Mesoporous Silica Particles

Integrated with All-Inorganic CsPbBr<sub>3</sub> Perovskite Quantum-Dot Nanocomposites (MP-PQDs) with High Stability and Wide Color Gamut Used for Backlight Display. *Angew. Chem., Int. Ed.* **2016**, *55*, 7924–7929.

(24) Dirin, D. N.; Protesescu, L.; Trummer, D.; Kochetygov, I. V.; Yakunin, S.; Krumeich, F.; Stadie, N. P.; Kovalenko, M. V. Harnessing Defect-Tolerance at the Nanoscale: Highly Luminescent Lead Halide Perovskite Nanocrystals in Mesoporous Silica Matrixes. *Nano Lett.* **2016**, *16*, 5866–5874.

(25) Malgras, V.; Henzie, J.; Takei, T.; Yamauchi, Y. Hybrid Methylammonium Lead Halide Perovskite Nanocrystals Confined in Gyroidal Silica Templates. *Chem. Commun.* **2017**, *53*, 2359–2362.

(26) Malgras, V.; Tominaka, S.; Ryan, J. W.; Henzie, J.; Takei, T.; Ohara, K.; Yamauchi, Y. Observation of Quantum Confinement in Monodisperse Methylammonium Lead Halide Perovskite Nanocrystals Embedded in Mesoporous Silica. *J. Am. Chem. Soc.* **2016**, *138*, 13874–13881.

(27) Liu, J.; Zhang, L.; Yang, Q.; Li, C. Structural Control of Mesoporous Silicas with Large Nanopores in A Mild Buffer Solution. *Microporous Mesoporous Mater.* **2008**, *116*, 330–338.

(28) Yang, J.; Siempelkamp, B. D.; Liu, D.; Kelly, T. L. Investigation of CH<sub>3</sub>NH<sub>3</sub>PbI<sub>3</sub> Degradation Rates and Mechanisms in Controlled Humidity Environments Using in Situ Techniques. *ACS Nano* **2015**, *9*, 1955–1963.

(29) Huang, S.; Li, Z.; Kong, L.; Zhu, N.; Shan, A.; Li, L. Enhancing the Stability of CH<sub>3</sub>NH<sub>3</sub>PbBr<sub>3</sub> Quantum Dots by Embedding in Silica Spheres Derived from TMOS in "Waterless" Toluene. *J. Am. Chem. Soc.* **2016**, *138*, 5749–5752.

(30) Sun, C.; Zhang, Y.; Ruan, C.; Yin, C.; Wang, X.; Wang, Y.; Yu, W. Efficient and Stable White LEDs with Silica-Coated Inorganic Perovskite Quantum Dots. *Adv. Mater.* **2016**, *28*, 10088–10094.

(31) Luo, B.; Pu, V. C.; Lindley, S. A.; Yang, Y.; Lu, L.; Li, Y.; Li, X.; Zhang, J. Z. Organolead Halide Perovskite Nanocrystals: Branched Capping Ligands Control Crystal Size and Stability. *Angew. Chem.* **2016**, *128*, 9010–9014.

(32) Zhang, F.; Zhong, H. Z.; Chen, C.; Wu, X. G.; Hu, X. M.; Huang, H. L.; Han, J. B.; Zou, B. S.; Dong, Y. P. Brightly Luminescent and Color-Tunable Colloidal CH<sub>3</sub>NH<sub>3</sub>PbX<sub>3</sub> (X = Br, I, Cl) Quantum Dots: Potential Alternatives for Display Technology. *ACS Nano* **2015**, *9*, 4533–4542.

(33) Bai, Z.; Zhong, H. Halide Perovskite Quantum Dots: Potential Candidates for Display Technology. *Sci. Bull.* **2015**, *60*, 1622–1624.

(34) Li, X. M.; Wu, Y.; Zhang, S. L.; Cai, B.; Gu, Y.; Song, J. Z.; Zeng, H. B. CsPbX<sub>3</sub> Quantum Dots for Lighting and Displays: Room-Temperature Synthesis, Photoluminescence Superiorities, Underlying Origins and White Light-Emitting Diodes. *Adv. Funct. Mater.* **2016**, *26*, 2435–2445.

(35) Ruan, L.; Shen, W.; Wang, A.; Xiang, A.; Deng, Z. Alkyl-Thiol Ligand-Induced Shape- and Crystalline Phase-Controlled Synthesis of Stable Perovskite-Related CsPb<sub>2</sub>Br<sub>5</sub> Nanocrystals at Room Temperature. *J. Phys. Chem. Lett.* **2017**, *8*, 3853–3860.

(36) Chiappim, W., Jr; Awano, C. M.; Donatti, D. A.; de Vicente, F. S.; Vollet, D. R. Structure of Hydrophobic Ambient-Pressure-Dried Aerogels Prepared by Sonohydrolysis of Tetraethoxysilane with Additions of N,N-Dimethylformamide. *Langmuir* **2014**, *30*, 1151–1159.

(37) Wang, Y.; Kalytchuk, S.; Zhang, Y.; Shi, H.; Kershaw, S. V.; Rogach, A. L. Thickness-Dependent Full-Color Emission Tunability in a Flexible Carbon Dot Ionogel. *J. Phys. Chem. Lett.* **2014**, *5*, 1412–1420.

(38) Colilla, M.; Darder, M.; Aranda, P.; Ruiz-Hitzky, E. Amino-polysiloxane Hybrid Materials as Carbon Composite Electrodes for Potentiometric Detection of Anions. *J. Mater. Chem.* **2005**, *15*, 3844–3851.

(39) Liu, C.; Yang, D.; Jiao, Y.; Tian, Y.; Wang, Y.; Jiang, Z. Biomimetic Synthesis of TiO<sub>2</sub>-SiO<sub>2</sub>-Ag Nanocomposites with Enhanced Visible-Light Photocatalytic Activity. *ACS Appl. Mater. Interfaces* **2013**, *5*, 3824–3832.

(40) Kim, Y. H.; Lee, D. K.; Cha, H. G.; Kim, C. W.; Kang, Y. S. Synthesis and Characterization of Antibacterial Ag-SiO<sub>2</sub> Nanocomposite. *J. Phys. Chem. C* **2007**, *111*, 3629–3635.

(41) Liu, C.; Yang, D.; Jiao, Y.; Tian, Y.; Wang, Y.; Jiang, Z. Biomimetic Synthesis of TiO<sub>2</sub>-SiO<sub>2</sub>-Ag Nanocomposites with Enhanced Visible-Light Photocatalytic Activity. *ACS Appl. Mater. Interfaces* **2013**, *5*, 3824–3832.

(42) Aslam, M.; Schultz, E. A.; Sun, T.; Meade, T.; Dravid, V. P. Synthesis of Amine-Stabilized Aqueous Colloidal Iron Oxide Nanoparticles. *Cryst. Growth Des.* **2007**, *7*, 471–475.

(43) Sharma, J.; Mahima, S.; Kakade, B. A.; Pasricha, R.; Mandale, A. B.; Vijayamohan, K. Solvent-Assisted One-Pot Synthesis and Self-Assembly of 4-Aminothiophenol-Capped Gold Nanoparticles. *J. Phys. Chem. B* **2004**, *108*, 13280–13286.

(44) Sun, P.; Zhang, H.; Liu, C.; Fang, J.; Wang, M.; Chen, J.; Zhang, J.; Mao, C.; Xu, S. Preparation and Characterization of Fe<sub>3</sub>O<sub>4</sub>/CdTe Magnetic/Fluorescent Nanocomposites and Their Applications in Immuno-labeling and Fluorescent Imaging of Cancer Cells. *Langmuir* **2010**, *26*, 1278–1284.

(45) Michalska, M.; Aboulaich, A.; Medjahdi, G.; Mahiou, R.; Jurga, S.; Schneider, R. Amine Ligands Control of the Optical Properties and the Shape of Thermally Grown Core/shell CuInS<sub>2</sub>/ZnS Quantum Dots. *J. Alloys Compd.* **2015**, *645*, 184–192.

(46) Shirasaki, Y.; Supran, G. J.; Bawendi, M. G.; Bulović, V. Emergence of Colloidal Quantum-Dot Light-Emitting Technologies. *Nat. Photonics* **2013**, *7*, 13–23.

(47) Dong, X.; Wei, L.; Su, Y.; Li, Z.; Geng, H.; Yang, C.; Zhang, Y. Efficient Long Lifetime Room Temperature Phosphorescence of Carbon Dots in a Potash Alum Matrix. *J. Mater. Chem. C* **2015**, *3*, 2798–2801.

(48) Zhang, Y.; Liu, X.; Fan, Y.; Guo, X.; Zhou, L.; Lv, Y.; Lin, J. One-Step Microwave Synthesis of N-Doped Hydroxyl-Functionalized Carbon Dots with Ultra-High Fluorescence Quantum Yields. *Nanoscale* **2016**, *8*, 15281–15287.

(49) Chirvony, V. S.; González-Carrero, S.; Suarez, I.; Galian, R. E.; Sessolo, M.; Bolink, H. J.; Martínez-Pastor, J. P.; Pérez-Prieto, J. Delayed Luminescence in Lead Halide Perovskite Nanocrystals. *J. Phys. Chem. C* **2017**, *121*, 13381–13390.

(50) Gabelloni, F.; Biccari, F.; Andreotti, G.; Balestri, D.; Checcucci, S.; Milanesi, A.; Calisi, N.; Caporali, S.; Vinattieri, A. Recombination dynamics in CsPbBr<sub>3</sub> nanocrystals: role of surface states. *Opt. Mater. Express* **2017**, *7*, 4367–4373.

(51) Wang, Y.; Zhi, M.; Chan, Y. Delayed Exciton Formation Involving Energetically Shallow Trap States in Colloidal CsPbBr<sub>3</sub> Quantum Dots. *J. Phys. Chem. C* **2017**, *121*, 28498–28505.

(52) Yang, G.; Fan, Q.; Chen, B.; Zhou, Q.; Zhong, H. Reprecipitation synthesis of luminescent CH<sub>3</sub>NH<sub>3</sub>PbBr<sub>3</sub>/NaNO<sub>3</sub> nanocomposites with enhanced stability. *J. Mater. Chem. C* **2016**, *4*, 11387–11391.

(53) Niu, G.; Guo, X.; Wang, L. Review of Recent Progress in Chemical Stability of Perovskite Solar Cells. *J. Mater. Chem. A* **2015**, *3*, 8970–8980.

(54) Kim, H.; Jang, H. S.; Kwon, B.-H.; Suh, M.; Youngsun, K.; Cheong, S. H.; Jeon, D. Y. In Situ Synthesis of Thiol-Capped CuInS<sub>2</sub>-ZnS Quantum Dots Embedded in Silica Powder by Sequential Ligand-Exchange and Silanization. *Electrochem. Solid-State Lett.* **2011**, *15*, K16–K18.

(55) Jang, E.; Jun, S.; Jang, H.; Lim, J.; Kim, B.; Kim, Y. White-Light-Emitting Diodes with Quantum Dot Color Converters for Display Backlights. *Adv. Mater.* **2010**, *22*, 3076–3080.

(56) Abe, S.; Joos, J. J.; Martin, L. I.; Hens, Z.; Smet, P. F. Hybrid Remote Quantum Dot/Powder Phosphor Designs for Display Backlights. *Light: Sci. Appl.* **2016**, *6*, e16271.

(57) Chen, H.-W.; Zhu, R.-D.; He, J.; Duan, W.; Hu, W.; Lu, Y.-Q.; Li, M.-C.; Lee, S.-L.; Dong, Y.-J.; Wu, S.-T. Going Beyond the Limit of an LCD's Color Gamut. *Light: Sci. Appl.* **2017**, *6*, e17043.

(58) Jun, S.; Lee, J.; Jang, E. Highly Luminescent and Photostable Quantum Dot-Silica Monolith and Its Application to Light-Emitting Diodes. *ACS Nano* **2013**, *7*, 1472–1477.